First-principles study of Au nanostructures on rutile TiO_2(110)

Tomasz Pabisiak and Adam Kiejna*
Institute of Experimental Physics, University of Wrocław, Plac M. Borna 9, PL-50-204 Wrocław, Poland
(Received 29 September 2008; published 11 February 2009)

We report systematic density-functional theory calculations of the structure and energetics of Au_n nanorows ($n=1-7$) and clusters ($n=1-12$) adsorbed on the defected (110) rutile surface. The calculations show that gold nanorows bind strongly to a missing-row defected TiO_2 surface with an adhesive binding energy of about 1.5 eV. The cohesive binding energy of Au atoms in a row amounts to about 2.5 eV/atom. An analysis of the gold row properties points to their metallic nature. The charge redistribution on adsorbed rows shows that all Au_n rows are negatively charged compared to the free-standing structures. The adhesive bonding of gold clusters to the vacancy defected bridging oxygen row at the TiO_2(110) is of covalent nature and is stronger than that of the Au rows. The cohesive energy per atom in a Au_n cluster is about 2.2 eV for the $n \geq 5$ clusters and is larger ($\sim 2.3-2.4$ eV) for smaller ones. We found that all clusters studied are negatively charged with about 1.1 electron charge. This charging shows only a weak dependence on the odd-even number of gold atoms forming a cluster.

DOI: 10.1103/PhysRevB.79.085411 PACS number(s): 68.35.−p, 68.43.Bc, 68.47.Gh, 73.22.−f

I. INTRODUCTION

The striking catalytic properties of dispersed gold nanoparticles on oxide supports discovered by Haruta *et al.*[1] have stimulated a lot of research on gold/oxide system. The experimental investigations have revealed that the catalytic activity of Au particles in CO oxidation is exceptionally high when gold is supported on reducible oxides such as TiO_2 and Fe_2O_3. Numerous studies of the Au/TiO_2 system suggested several factors that can contribute to the special catalytic performance of gold particles on titania: bilayer structure of Au islands,[2,3] perimeter sites of the nanoparticle,[4] high concentration of low-coordinated sites,[5,6] or charge transfer from the support.[7,8] Small aggregates offer configurations of low-coordinated edge and corner atoms, which cannot be found on extended surfaces. Thus, it is commonly believed that the main factors determining the catalytic activity of the gold particles are the size and shape of the gold particles and the oxide support.

In the last ten years first-principles electronic structure calculations based on density-functional theory (DFT) have been extensively used to provide information on the optimum size and stable adsorption sites of gold nanoparticles on the TiO_2(110) single-crystal surface. The earliest DFT calculations concentrated on the adsorption of single Au atoms on stoichiometric rutile (110) surface represented by unrelaxed[9] and relaxed[10] slabs of several layers of TiO_2. The site atop the fivefold coordinated (5*c*) titanium atom was identified as the most stable.[9,10] Cluster model calculations,[11] as well as calculations for relaxed rutile slabs,[12] in turn, predicted Au adsorption over the twofold coordinated bridging oxygen (O^{br}). At higher coverage adsorption atop the Ti(5*c*) atom was found to be favored.[12] As shown by many recent first-principles simulations, the geometric and electronic structures of clean oxide surfaces are significantly modified by the presence of surface defects such as oxygen vacancies (for a review see Ref. 13). Consequently, subsequent DFT studies have considered gold adsorption on the defected TiO_2(110) and demonstrated that the binding of Au to an oxygen vacancy sites is substantially stronger than to the stoichiometric surface.[14–17] The O^{br} vacancy was found to be the most stable site, both for the adsorption of Au monomers[14–16] and dimers.[15] It was also found that the greater the degree of reduction in the rutile support the stronger the Au binding.[15] The role of O^{br} vacancies as the active nucleation sites for Au particles was confirmed by scanning tunneling microscopy (STM) measurements, which showed that a single O^{br} vacancy can bind three Au atoms on average.[16] DFT calculations for a monolayer of Au on a perfect rutile surface and on a TiO_2(110) surface with O^{br} vacancies forming a missing-row structure[17] showed negligibly small binding between Au and a perfect rutile surface, while in the presence of vacancies a binding energy of about 1.6 eV/defect was found. Similar conclusions about much stronger binding of single Au atom to the O^{br} defected than to the stoichiometric surface were reached by other DFT calculations.[18,19]

For larger supported Au aggregates, such as clusters[20,21] or nanorods,[8] first-principles calculations are relatively seldom. Usually such systems were considered in the context of CO oxidation on the surface of the particle, without discussing, however, the energetics of their interaction with the support. The first systematic comparison of calculated structures and bonding of Au_n clusters ($n=1-4$) anchored at a single vacancy on the TiO_2(110) support was presented by Pillay and Hwang.[22] They confirmed the preference of Au for binding to the O^{br} vacancy sites and showed that the Au adsorption energy oscillates with the number of atoms in a particle. Based on experimental observation[23,24] that low-dimensional Au structures can be formed in a controlled manner on a TiO_2(110) surface, using ordered O^{br} vacancies, we have demonstrated with first-principles calculations[23,24] a strong bonding of Au on O^{br} vacancies and formation of stable 1–3 Au atom wide chains, extending along the O^{br} vacancy line. Such tendency for the O^{br} vacancies to arrange themselves in close-packed linear configurations at high vacancy concentrations has been confirmed by recent Monte Carlo simulations.[25] A detailed analysis of the calculated structural and binding properties (including the charge exchange between the cluster and the support) of the Au_n clusters (*n*

$=1-7$) adsorbed on the reduced[26,27] and stoichiometric[28] $TiO_2(110)$ surfaces has been recently presented by Chrétien and Metiu.[26–28] All these calculations provide strong evidence that on the rutile $TiO_2(110)$ surface the binding of gold particles to surface defects is substantially stronger than to the stoichiometric surface. However, Wang and Hammer[29] considered stable Au_7 cluster adsorbed at $TiO_2(110)$ and reported weaker binding to the vacancy defected than to the stoichiometric surface. In a combined STM and DFT study of the bonding of Au_n particles ($n=1-5,7$) to the $TiO_2(110)$ surface, Matthey *et al.*[30] recently showed that the Au bonding to nondefected, oxidized surface is the most favorable. Thus, the role of oxygen vacancies in the stabilization of Au particles on oxide surfaces, under real reaction conditions, has been debated.[30]

In this work we performed density-functional theory calculations to examine the adsorption properties of small Au aggregates (rows and clusters) of a size ranging from a monomer to a dozen of Au atoms per cell on a partially reduced rutile $TiO_2(110)$ surface. Thus, our previous results[23,24] for the monomer, dimer, and trimer Au rows are extended to higher Au coverages and are supplemented by the results for clusters in order to investigate the effect of the shape and size of the Au particles. The discussion is focused on the structure and bonding of the one-dimensional Au rows formed on the missing-row defected $TiO_2(110)$ surface and their comparison with the respective properties of Au clusters adsorbed on the partially defected bridging O row. As recent experiments have shown the reactivity of Au nanoparticles can be considerably increased by charging the particles negatively. Therefore we also examine electron-charge transfer and discuss the charging of rows/clusters and its dependence on the aggregate size. Results from this study give valuable insight into the nature of the Au-Ti bond, the role of the amount of deposited metal on the electronic properties, and the growth behavior of Au nanostructures on $TiO_2(110)$.

II. METHODS OF CALCULATION

The calculations have used the Vienna *ab initio* simulation package[31,32] based on the density-functional theory. The exchange-correlation energy is treated in the Perdew-Burke-Ernzerhof (PBE) version[33] of the generalized gradient approximation (GGA) functional. We used a spin polarized approach because of the unpaired electrons at the defected rutile surface. A plane wave basis set including components with energy of up to 400 eV is applied. The electron ion-core interactions are described by the projector augmented-wave (PAW) method with a scalar-relativistic treatment for gold.[34] The PAW method[35] is a frozen core approach which uses the exact valence wave-functions instead of pseudowave functions. We apply the theoretical lattice parameters of rutile TiO_2 structure ($a=4.669$ Å, $c=2.958$ Å, and $u=0.3046$) which were reoptimized to account for the GGA-PBE functional, compared to those determined by us previously.[36]

The rutile $TiO_2(110)$ surface was modeled by periodic slabs separated by a vacuum layer. To consider adsorption of the Au rows we applied a 1×2 surface unit cell and slabs consisting of five trilayers of TiO_2, separated by a thick vacuum layer of 13 Å for monomer, 16 Å for a dimer, and 22 Å for thicker rows in order to keep the separation between slabs larger than 7.0 Å. The Au rows were grown in place of the bridging oxygen vacancy rows created by removing every second O^{br} row. Symmetric slabs were considered, with gold atoms adsorbed on both sides of a slab. The positions of all atoms were optimized until the forces on atoms were smaller than 0.02 eV/Å. To study adsorption of Au clusters we used a thinner slab of three TiO_2 trilayers and a larger 4×2 surface unit cell. These resulted in 144 atoms in an undisturbed supercell. A vacuum width of 16 Å was applied that allowed to keep the distance between the atoms of the neighboring slabs larger than 8 Å. The Au clusters were adsorbed on one side of the slab. Atoms of the outermost trilayer of the $TiO_2(110)$ support and all adsorbate atoms were relaxed, with a less strict condition for the Hellman-Feynman forces on atoms (<0.05 eV/Å). The atoms of the middle TiO_2 layer were frozen in the positions optimized for a clean, defected surface, whereas those of the bottom layer were frozen in their bulk positions. For the Brillouin-zone integrations a $1\times4\times1$ set of the Monkhorst-Pack[37] special k points was applied for the adsorption of rows. In the case of adsorption of clusters, because of the large unit cell, the Brillouin zone was sampled only at the Γ point. To calculate the local density of electronic states we used the tetrahedron method and denser k-point meshes ($2\times4\times1$ for the Au rows and $2\times2\times1$ for clusters) with the Γ point included. To improve the convergence of the solutions a Gaussian broadening of the Fermi surface of 0.1 eV was applied for all systems considered.

The energy of adhesion (attachment) of the nanostructure (row or cluster) adsorbed symmetrically on both sides of the slab was calculated according to

$$E_{\mathrm{adh}} = (E^{\mathrm{Au}_n/\mathrm{sub}} - E^{\mathrm{sub}} - 2E^{\mathrm{Au}_n})/2, \tag{1}$$

where $E^{\mathrm{Au}_n/\mathrm{sub}}$ is the total energy of the Au covered slab, E^{sub} represents the energy of the relaxed bare-support slab, and E^{Au_n} is the energy of the free Au_n row/cluster of n atoms calculated in the same supercell as the adsorbate-substrate system. For a one-side adsorption of clusters the factor 2 was replaced by 1.

The adsorption binding energy (per Au atom), or (for $n\geq2$) a cohesive energy for the adsorbed nanostructure, was calculated from the following expression:

$$E_b = (E^{\mathrm{Au}_n/\mathrm{sub}} - E^{\mathrm{sub}} - 2nE^{\mathrm{Au}})/2n, \tag{2}$$

where E^{Au} is the energy of an isolated Au atom (calculated in a large supercell). Note that though for $n=1$ Eqs. (1) and (2) are formally identical, in general, they will give different results because E^{Au} is calculated in different supercells.

To analyze the electron-charge density distribution in the system we examined the difference $\Delta\rho(\mathbf{r})$ in the electron-charge density of the complete adsorption system and their isolated components as follows:

$$\Delta\rho(\mathbf{r}) = \rho^{\mathrm{Au}_n/\mathrm{sub}}(\mathbf{r}) - \rho^{\mathrm{sub}}(\mathbf{r}) - \rho^{\mathrm{Au}_n}(\mathbf{r}), \tag{3}$$

where $\rho^{\mathrm{Au}_n/\mathrm{sub}}(\mathbf{r})$ is the electron-charge density of the complete adsorption system, and the latter two components represent, respectively, the density of the bare substrate, and the

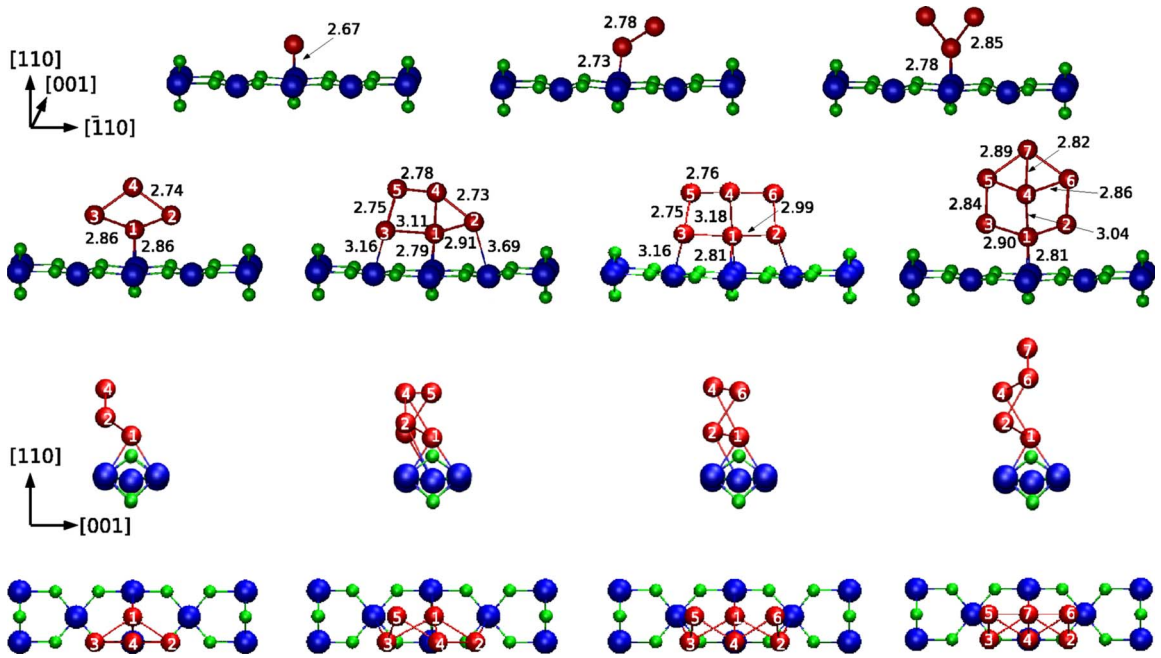

FIG. 1. (Color online) Front views (along the rows) of the optimized final configurations (first and second rows) of Au_n rows ($n=1-7$) on the missing-row 1×2 surface cell of $TiO_2(110)$. Gold atoms are represented by the medium-size red (gray) balls (numbered in white), the largest blue (darkest) balls represent Ti, whereas the smallest green (light gray) balls represent oxygen atoms. Only the atoms of the topmost trilayer of the (110) oriented TiO_2 slab are displayed. The noninteger numbers show the Au-Au and Au-Ti bond lengths (in angstrom). The third and bottom rows display, respectively, side view along the $[\bar{1}10]$ direction and top view of the $n=4-7$ gold rows. For the top view of $n=1-3$ rows consult Fig. 4 of Ref. 23.

free adsorbate calculated in the configuration corresponding to that on the relaxed Au/TiO_2 system.

In order to quantify the electron-charge redistribution on atoms in the adsorbed Au_n aggregates, we calculated the electronic charges on atoms by using the method proposed by Bader.[38] The analysis of the electron-charge transfer to/from the Au_n clusters or rows requires calculation of the charge on the gold atoms of the adsorbed Au_n aggregate and then subtraction of the corresponding charge of the free aggregate. To this end we applied the numerical implementation of the Bader method developed by Henkelman *et al.*[39]

III. RESULTS AND DISCUSSION

A. Au rows

1. Energetics

Our previous work[23,24] for the Au_n rows, $n=1-3$, has shown that the monomer (or Au_1) rows are strongest bound when placed in the empty O^{br} sites on the missing-row 1×2 surface. This configuration appeared to be the most stable of all single Au rows on the stoichiometric, and defected surfaces, and formed a sort of support for anchoring the additional Au rows. The Au monomer, dimer, and trimer rows were formed on the defected 1×2 surface by placing Au atoms in various sites around the missing O^{br} row.[24] The optimized configurations, giving the energetically most stable structures, are displayed in Fig. 1. The initial trimer-row geometry was adopted as the starting point for building the initial configurations of four to seven Au_n rows which subsequently were optimized to determine the energetically most stable configuration. In this sense our search for the energetically best structures was limited by the results of optimization performed for the three lowest isomers. It is possible that the structures considered by us do not represent the minimum-energy configurations without this restriction. The resulting configurations are summarized in Fig. 1, where the corresponding Au-Au and Au-Ti bond lengths are also shown. The front view of the structures presented in two upper rows of Fig. 1 looks planarlike in the plane normal to the [001] direction; however, for $n\geq3$ the atoms are shifted within the unit cell in the [001] direction (see the third and bottom rows in Fig. 1). The Au_n rows considered by us show some similarity to the one-dimensional Au_5 rods adsorbed atop the O^{br} atoms of stoichiometric surface, which were considered by Molina *et al.*[8] There, the Au rods were assumed to have an fcc structure from the outset and only 30% of atoms forming the rod were fully relaxed while the remaining kept the fcc structure. The Au rows calculated by us have different structure resulting from the atom by atom growth. However, an inspection of the numbers for the interatomic distances in the rows (Fig. 1) shows that they, as well as their repeat distance along the rows (2.96 Å), are close to the nearest-neighbor distance (2.88 Å) in the bulk of fcc Au.

The variations in the calculated adhesion energy, binding energy per adsorbed Au atom, and work function, with the size of the investigated rows are displayed in Fig. 2. The Au atoms adhere rather strongly (0.8 to 1.55 eV) to the defected $TiO_2(110)$ support, the adhesive bond being strongest for the Au_1 and Au_2 rows (1.52–1.55 eV) and weakest for the Au_4

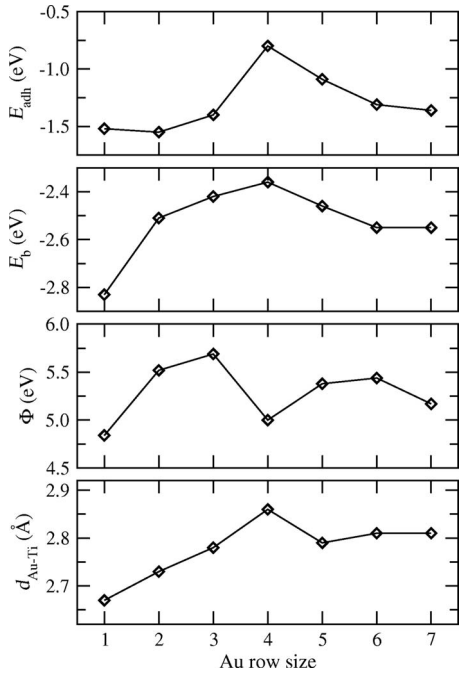

FIG. 2. The adhesion energy E_{adh}, adsorption binding energy per atom E_{coh}, and work function, Φ, of the Au_n rows adsorbed on the missing O^{br} row of the TiO_2(110) surface. The lowest panel displays the bond length between the bottom Au and the nearest surface Ti atom.

rows (0.80 eV). The latter is also reflected in the largest distance of the Au_4 row from the surface support atoms. The adhesive binding energy of the monomer row is by 0.4 eV smaller than that calculated, using a different DFT code, for the completely reduced surface (1.90 eV).[18] There is a large contribution to the adhesion energy resulting from the structural relaxation caused by the adsorbate. By substituting for the E^{sub} term in Eq. (1) the energy of the bare-support slab, calculated with the atomic positions of Ti and O frozen at those corresponding to the adsorbate-substrate system but now with the Au atoms removed, one gets adhesive energies of the Au_n rows larger by about 0.5 eV.

The binding energy of the Au rows, which for $n \geq 2$ gives information on the cohesive binding of the Au atoms in the row, initially decreasing with the number of atoms forming the row, from 2.83 eV for the Au_1 row, is weakest (2.36 eV) for the Au_4 row and then increases by 0.1–0.2 eV to saturate at 2.55 eV for $n \geq 6$. It is worth noting that this binding is by about 1.3–1.8 eV weaker than that of the Au atomic chains on transition metal (Mo and Ti) surfaces.[40] The binding energy for the Au_1 row is in very good agreement with that calculated, using the same code, for the missing-row surface (2.78 eV) (Ref. 14) and for the Au row formed on a fully reduced surface (2.86 eV) (Ref. 15) represented by five TiO_2 trilayers, with a slightly different GGA functional.

The adsorption-induced change in the work function is another quantity of interest. Upon Au adsorption, the work function is substantially enhanced (from 0.32 to 1.17 eV) compared to the clean, missing-row TiO_2(110) surface (4.52 eV), with the largest increase for the Au_3 row, where it reaches 5.69 eV. It decreases to 5.0 eV for the Au_4 row

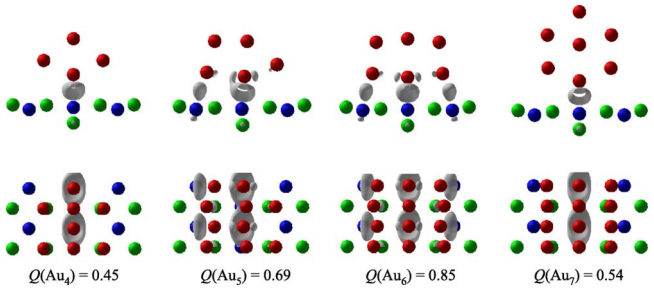

FIG. 3. (Color online) Front and top views of the surfaces of constant electron-charge-density change upon adsorption of four to seven Au atom rows. Only isosurfaces (0.03 $e/Å^3$) of the electron-charge gain are displayed. Blue (darkest), green (light gray), and red (gray) balls represent Ti, O, and Au atoms, respectively. The isosurfaces for $n=1-3$ rows were presented in Ref. 23. The numbers $Q(Au_n)$ give the total Bader charges (in units of the electron charge e) gained by the rows. The corresponding charges for the Au_1, Au_2, and Au_3 rows are 0.56, 0.58, and 0.57e, respectively.

which is attributed to the sharper edge formed by the top Au in the rows of $n=1$, 4, and 7 atoms (see Fig. 1). The electron-charge transfer from the TiO_2 support to the Au_n row (see below) leads to an increase in the surface dipole moment and results in a higher work function for the adsorbed Au_n rows. Note that in all cases the work function is still much smaller than that of the stoichiometric clean surface (6.98 eV). The latter value is about 1.5 eV larger than that reported in experimental work.[41] The presence of point defects (vacancies) in surface and/or subsurface layers results in work function values of 5.0–5.6 eV,[42] which compare well with those measured experimentally for stoichiometric surfaces.[41,43] The energetic properties of the Au rows (Fig. 2) do not show any clear trend with respect to the odd-even number of atoms in the adsorbed structure.

The Au-row-substrate distance (the Au-Ti bond length) correlates with the variation in the adhesion energy with the number of Au atoms in the row. The Au-Au distance in the [001] direction (along the row) is 2.96 Å (and is determined by the value of the rutile lattice parameter c).

2. Electronic properties

In order to gain insight into the charge distribution difference in the system caused by the adsorbate, we have calculated electron-density changes $\Delta\rho(\mathbf{r})$ as defined by Eq. (3). The positive values of the isocharge surfaces show the regions of the electron-charge gain upon Au bonding. The isocharge surfaces of the electron-density difference for Au_n rows ($n=4-7$) are displayed in Fig. 3. They are very similar to the corresponding plots for Au rows with $n=1-3$, which were presented by us previously.[23,24] Similar to the Au_1-Au_3 rows, the bonding of Au is mainly to the substrate sixfold coordinated Ti(6c) atoms below. For the Au_5 and Au_6 there is also bonding of the bottom Au to the Ti(5c) atoms of the substrate. The accumulation of the electron-charge density between the substrate Ti and adsorbate Au atoms indicates a predominantly covalent character of bonding. However, the spatial extent of this electron-charge gain is not limited only to the space between the binding Au of the Au_n row and the

Ti atoms of the support but forms a stripe of accumulated one-dimensional electron gas that extends along the Au rows in the [001] direction. Interestingly, the delocalization of this charge is not increasing with the number of Au atoms in the row.

More quantitative information on the electron-charge transfer to/from adsorbed atoms can be obtained from a Bader charge analysis.[39] Our previous calculations[23,24] of the electron charge confined in the Wigner-Seitz spheres around the considered atoms showed that for the Au_1-Au_3 rows the bonding between Au and surface atoms is determined by electron transfer from the localized *d* states to the more extended *s* states. The changes in the total Bader charges on the adsorbed Au_n rows calculated in this work are shown in Fig. 3. To maintain consistency in our description with that of the electron-density differences presented above, we use the convention that a positive number indicates that the Au aggregate gains electronic charge when adsorbed. Note that it is opposite to the convention applied in Ref. 26.

Our calculations show that for all rows considered the row gains electron charge when it is adsorbed; i.e., all rows become negatively charged. This is in line with the conclusion of previous studies[14,18] about electron transfer from the substrate to Au on the O-deficient TiO_2 surface. The total electron-charge gain of the Au_n rows varies between $0.45e$ per row unit for the Au_4 row and $0.85e$ for the Au_6 row. For the $n=1-3$ rows the accumulated charge is almost constant at $\sim 0.57e$/row unit. It decreases to $0.45e$ for Au_4 then rises for Au_5 and achieves maximum for Au_6 to decrease again to $0.54e$ for the Au_7 row. Au accepts some electrons that the oxygen left behind in the vacancy site. In agreement with the electron-density difference plots (Fig. 3), we find that for all the structures most of the electron-charge gain (80%–86% for Au_2-Au_4, 73% for Au_5, 58% for Au_6, and 78% for Au_7) can be ascribed to the Au atom adsorbed in the O^{br} vacancy row that forms the "foot" on which the remaining Au atoms stand. The major part of the electron charge transferred ($\sim 0.3e$) originates from the oxygen vacancy that bridges sixfold coordinated Ti atoms of the $TiO_2(110)$ basal plane. After an O^{br} vacancy is created the electrons that formed the Ti-O-Ti bonds are localized on two Ti($6c$) atoms. The latter donates 53%–63% of the total electron charge transferred from the substrate to the Au_1-Au_4 and Au_7 rows and, respectively, 47% and 41% of that transferred to Au_5 and Au_6. The second principal electron donors are two threefold coordinated oxygen atoms lying on the two sides of the O^{br} vacancy row in the basal $TiO_2(110)$ plane, which donate 20%–25% of the total electron charge transferred. The higher charge gain observed for the Au_5 and Au_6 rows is related to the formation of extra bonds between the Au aggregate and one or, in case of the Au_6, two Ti($5c$) atoms of the substrate basal plane (cf. Fig. 3). Thus one can conclude that the amount of electron charge transferred to the Au rows from the TiO_2 surface of the missing-row type is approximately constant, regardless of the number of Au atoms that form the row. The extra charges observed on the flatter Au_5 and Au_6 structures are transferred from the Ti($5c$) atoms.

As already mentioned above, the differences of the electron-charge-density distribution shown in Fig. 3 suggest metallic properties of the Au rows. In Fig. 4 we present the evolution of the local density of states (LDOS) on the Ti and O atoms of the top TiO_2 trilayer and on the Au adatoms in the vicinity of the Fermi level. The figure displays the local density of all electronic states, but it should be noted that in all cases considered the LDOS is dominated by the *d* states.

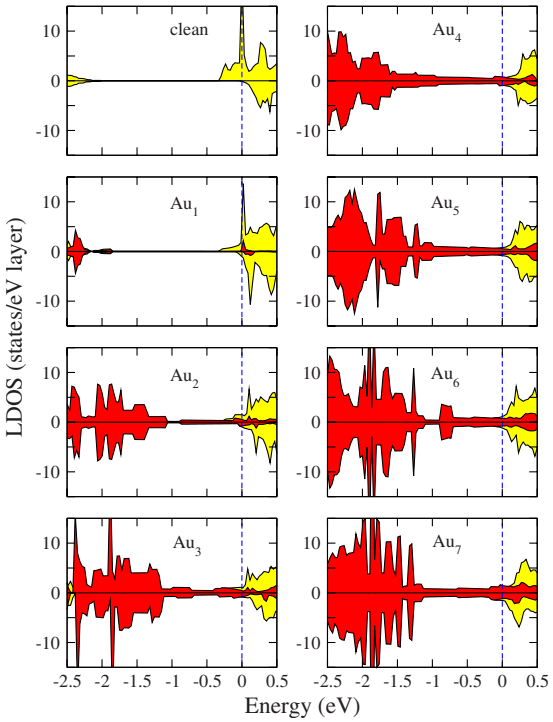

FIG. 4. (Color online) Evolution of the local density of states on the 1×2 missing-row $TiO_2(110)$ surface with the adsorption of the Au rows. Only the energy window close to the Fermi level (set as zero) is shown. Positive and negative values represent the spin-up and spin-down polarized electron states. The states of the top $TiO_2(110)$ layer atoms are plotted in yellow (gray), while red (dark gray) color marks the LDOS on the Au atoms.

The LDOS plots demonstrate (Fig. 4) that the spins of both even- and odd-numbered rows are paired. Furthermore, an inspection of the LDOS on the Au atoms shows the disappearance of the energy gap and a growing density of the occupied states close to the Fermi level, which indicates metallic character of the Au stripe.

B. Au clusters

1. Energetics

Clusters consisting of 1 to 12 Au atoms were placed in the 4×2 surface cell representing the defected $TiO_2(110)$ surface. The idea is to study the process of growth of the surface clusters, starting from the Au monomer to a dozen of Au atoms, which includes the Au_{10} configuration that was considered by Remediakis *et al.*[20] in their studies of CO oxidation on Au clusters. The initial configurations of the clusters with $n=1-3$ Au atoms were chosen in the empty O^{br} sites. First, three of four atoms of every second [001]-oriented surface O^{br} row, contained in the 4×2 unit cell, were removed in order to attain a ratio of 3–4 Au atoms per vacancy in the final cluster structures reported in an experimental study.[16]

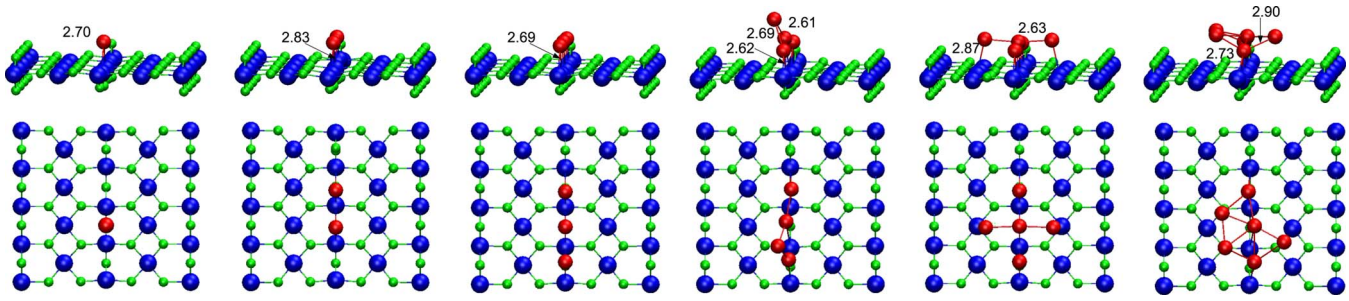

FIG. 5. (Color online) Side and top views of the optimized configurations of adsorbed Au_n clusters ($n=1-6$) on the defected $TiO_2(110)$ surface. Au atoms are represented by the medium-size red balls, the largest blue balls represent Ti, whereas the smallest green ones represent oxygen atoms. The numbers show the Au-Au bond lengths (in Å).

The Au atoms were adsorbed in the missing oxygen sites (Fig. 5). Single Au atom was placed either in the central position of the trivacancy O^{br} row ($1a$ site) or at the $1b$ site that is next to the only O^{br} atom that remained in the [001] oriented row. The second and third Au atoms filled the remaining O^{br} vacancy sites. As a result, in the O^{br} row [001] direction a linear Au cluster was formed in place of the three vacancy sites, separated by one O^{br} atom from the clusters in the neighboring cells. Thus for all clusters considered the distance between the cluster and its periodic replica in the [001] direction was only slightly shorter than 6 Å. Additional Au atoms were placed subsequently in different sites around the linear basis structure that was formed by Au_3 atoms sitting in the three O^{br} vacancy sites along the [001] directions. Thus all $n>3$ Au_n clusters bond through these three Au atoms adsorbed in place of the missing O^{br} atoms. The optimized, final configurations of the adsorbed Au_n clusters ($n=1-12$) on the defected $TiO_2(110)$ surface are displayed in Figs. 5 and 6.

Before we start the discussion of the resulting structures, we should note that they were obtained only within a very constrained search for a stable configuration. However, even for the free clusters the problem of determining the configuration of the lowest energy isomers is not trivial. For the relatively small Au clusters ($n\leq 12$) considered by us, DFT calculations predict that planar structures are lower in energy than nonplanar (three-dimensional) ones.[44,45] The calculated binding energies for a total of more than 100 two-dimensional and three-dimensional Au clusters showed that for $n\leq 12$ the planar structures are most stable.[44] The difference in the stability varies within $\simeq 0.2$ eV and is $\simeq 0.05$ eV for $n\geq 8$. For supported clusters the substrate plays an important role and nonplanar clusters may become more stable. Interestingly, DFT calculations for Au_n clusters ($n\leq 10$) have shown[45] that planar clusters when supported on oxide surfaces (MgO and anatase TiO_2) keep their planar conformation and prefer the orientation perpendicular to the surface. Besides, the stability of the supported clusters was greatly increased by the presence of oxygen vacancies. It should be stressed, however, that locating a global minimum for supported Au clusters of larger size is not possible using only DFT calculations.

The calculated adhesion energy, binding energy per adsorbed Au atom, and work functions of the Au_n clusters ($n=1-12$) adsorbed on the defected $TiO_2(110)$ surface are shown in Fig. 7 as a function of cluster size. The interaction of Au with oxygen vacancies on the defected surface is much stronger than with the stoichiometric surface.[14,15,23] When discussing the energies presented in Fig. 7, and making comparisons with the results for Au rows, one has to remember that the results for clusters were calculated for a thinner and not completely relaxed $TiO_2(110)$ slab consisting of only three rutile layers. Thus, a direct comparison of the absolute values of the calculated energies can be made only qualitatively. A quantitative comparison of the energy trends can be made only for each system (rows or clusters) separately.

Inspection of the values displayed graphically in Fig. 7 shows that, in general, the calculated adhesion energy for Au clusters is on average two times larger than that of the rows. The weakest adhesive bond is observed for the monomer (2.31 eV) and the Au_7 cluster (2.50 eV), whereas the strongest one appears for the Au_5 (4.52 eV) and Au_8 clusters (4.01

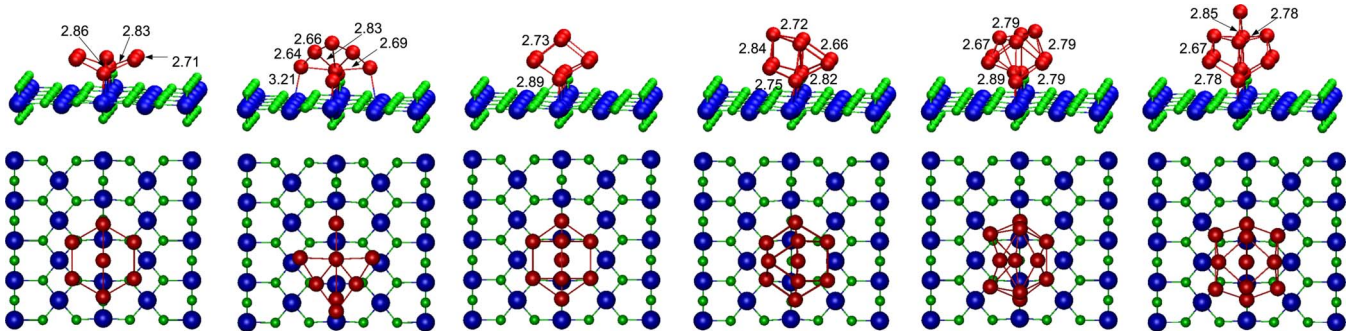

FIG. 6. (Color online) Same as in Fig. 5 but for the $n=7-12$ gold clusters.

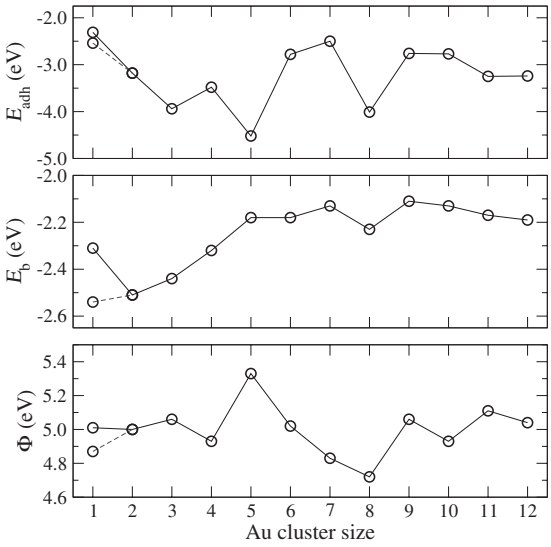

FIG. 7. Adhesion energy E_{adh}, adsorption binding energy per atom E_{coh}, and work function, Φ, of the Au_n clusters adsorbed on the defected $TiO_2(110)$ surface. The lower values for E_{coh} and Φ correspond to the 1*b* placement of the Au atom (cf. text).

eV). This enhanced adhesive energy results mainly from the enhanced structural relaxation contribution. Note that only the topmost-layer substrate and adsorbate atoms are allowed to relax upon cluster adsorption. To separate the role of this contribution, extra calculations for E_{adh} were performed with the E^{sub} term in Eq. (1) calculated for the cluster-substrate configuration but with all Au atoms removed while keeping the Ti and O positions frozen. They yield an adhesive energy stronger by 0.5 eV (Au_1) to 1.5 eV (Au_5), which gives an estimate of the relaxation energy contribution to the bond. Consequently, one can expect that for a completely relaxed system the adhesive energy of cluster will be reduced further and may attain the magnitudes not much different from those determined for the Au rows. Thus, the higher adhesive energies calculated for clusters do not necessarily mean that clusters adhere stronger than rows in a fully relaxed system. This is supported by the smaller values of the calculated difference between the E_b values of the rows and clusters (see below), which is less sensitive to the relaxation effects.

Additional information on the energy of the growth of the cluster can be estimated from the association energy needed to form an *n*-atom cluster from a single Au atom, which is given by: $E_{as}=E^{Au_n/sub}+E^{sub}-E^{Au_1/sub}-E^{Au_{n-1}/sub}$, where all the energy components are defined in Sec. II. The E_{as} quantity is very often used in analyzing the energetics of free as well as supported clusters.[46] It should be noted that in the cases considered by us E_{as} gives the energy to associate a Au atom that is adsorbed in the linear trivacancy on another surface (one cluster in supercell). The association of subsequent atoms to the nucleation site, which is served by a single Au atom in the trivacancy line, can be endothermic (positive energy value), exothermic (negative value), or neutral process. The energies involved both in endothermic or exothermic processes of nucleation of clusters do not exceed 1.15 eV, typically being of some tenths of eV, which is in good agreement with the numbers reported in Ref. 16.

The adsorption binding energy per adsorbed atom in a cluster (Fig. 7) shows a different trend compared to that observed in Au rows (Sec. III A). It amounts to 2.31 and 2.54 eV for the 1*a* and 1*b* monomers, respectively, increases to 2.51 eV for the dimer, and then stabilizes at about 2.10–2.20 eV in the larger clusters. Thus, it is by ~0.4–0.3 eV weaker than in Au rows and by 0.2–0.1 eV smaller than the bonding energy (per bond) of the free Au dimer.[44] The binding energies per Au atom in the dimer and the linear trimer are twice as large as in the free clusters, whereas the Au-Au distance in the adsorbed dimer and trimer is increased, respectively, to 2.90 and 2.71 Å, compared to 2.53 and 2.58 Å in free clusters.[44] Though not very regular, there is a weak oscillation in the cohesive binding energy with the number of atoms in a cluster; E_{coh} is generally smaller when the number of Au atoms is even.

Our result for the binding energy of Au_1 agrees very well with the calculations for the Au monomer adsorbed in place of a single vacancy (2.38 eV) (Refs. 14 and 15) and is about 0.6 eV higher than that reported in Ref. 22. Iddir *et al.*[19] found the binding energy of Au at the O^{br} site in the 2×1 and 4×2 cells of 2.18 and 2.03 eV, respectively, whereas Wahlström *et al.*[16] reported 2.0 eV for a Au monomer when calculated in a smaller 2×1 cell. In all these papers a different GGA energy functional was applied (PW91),[47] and the electron interactions with the ion cores were represented by ultrasoft pseudopotentials instead of the PAW potentials employed in this work.

For the Au_2 structure adsorbed in two adjacent O^{br}-vacancy sites of the missing-row 3×2 surface, the cohesive binding energy of Au was reported[15] to be 3.0 eV (and the Au-Au distance of 3.34 Å). The binding of Au_2, Au_3, and Au_4 clusters anchored to a single O^{br} vacancy was calculated to be weaker: 1.36, 2.04, and 1.90 eV, respectively.[22,48] Note, however, that from all the considered configurations, only the dimer structure was aligned in the [001] direction. The linear trimer and the Y-shaped tetramer structures were aligned normal to the [001] oriented O^{br} row. Some other vacancy ordering patterns were considered by Vijay *et al.*[15] They noticed that for a monomer and dimer adsorption the greater the degree of reduction in the substrate the stronger the binding. Very recently Chrétien and Metiu[26,27] considered adsorption of $n=1-7$ clusters, including the $n=1-4$ configurations discussed earlier by Pillay and Hwang,[22,48] bound to a single O^{br} vacancy. The binding energies reported by them for $n=1-7$ are between 1.00 and 2.08 eV. For $n=1-4$ their values are in line with those of Refs. 22 and 48; while for $n=5$, 6, and 7, they are, respectively, 1.60, 1.00, and 1.72 eV. Compared to our results for different Au_n clusters adsorbed at a trivacancy (Fig. 7) these energies are about 0.5–1.0 eV smaller. There are two reasons for this large difference. First, our clusters differ from those considered in Ref. 27. The main difference, however, is related to the fact that Au binds more weakly to more isolated vacancy.[15] Even lower values of the cohesive binding energy for $n=1-5,7$ clusters adsorbed at a single O^{br} vacancy were reported by Wang and Hammer[29] and Matthey *et al.*[30] They found that the cohesive binding of the most favorable planar Au_n clusters ($n=1-5,7$) is in the energy range of 0.31–1.41 eV, which is about 0.5 eV weaker than for the structures

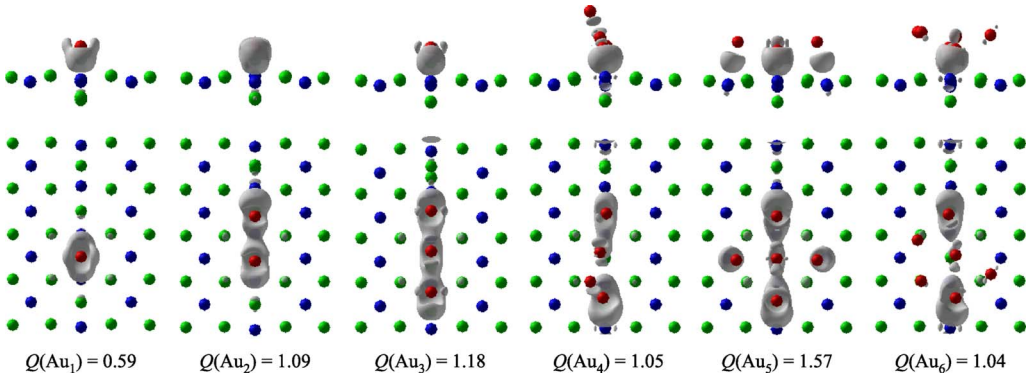

FIG. 8. (Color online) Side and top (lower row) views of the surfaces of constant electron-charge-density change upon adsorption of Au_n clusters ($n=1-6$). Only isosurfaces of the electron-charge gain, corresponding to 0.03 $e/Å^3$, are displayed. Blue (darkest), green (light gray), and red (gray) balls represent Ti, O, and Au atoms, respectively. The numbers $Q(Au_n)$ give the amount of electron charge gained by the cluster.

considered in Ref. 27 and about 1 eV less than for the structures considered by us (Fig. 7). The major part of this difference should originate from different configurations of the low-energy clusters considered in these studies and, additionally, is affected by the larger number of vacancies considered in our study. The binding energy of the Au_{10} cluster adsorbed at a trivacancy that was considered by Remediakis *et al.*[20] was not reported.

Upon cluster adsorption, the work function of the $TiO_2(110)$ surface does not change much, compared to that of the clean defected surface with partially removed O^{br} row (4.86 eV), and is in the range of 4.72–5.33 eV. In general, the work function oscillates (though not very regularly) with n, similar to the electron affinity and the ionization potential of unsupported Au clusters.[49] For smaller clusters ($n=1-4$) and the largest ones ($n=9-12$) the work function oscillates around 5.0 eV. The work function is on average smaller by 0.5 eV than that for the Au rows. It is largest (5.33 eV) for the Au_5 cluster that forms a symmetric structure which is "blunt" ended compared to other clusters protruding sharply from the surface. In addition, this flattened structure is characterized by an increased surface dipole layer due to the relatively large electron-charge transfer to the Au cluster.

2. Electronic properties

The calculated surfaces of constant electron-density difference induced by the Au_n clusters ($n=1-12$) are displayed in Figs. 8 and 9. They show that, similar to the Au rows, Au binds mainly to the underlying sixfold coordinated Ti atoms. For the flattened Au_5 cluster there is also bonding to the Ti($5c$) atoms of the support. The differences of the electron-charge density indicate the covalent features of this bonding. The bonding charge is more localized compared to the case of the Au rows (cf. Fig. 3) and is limited to the regions close to the bonding atoms. This is reflected in higher values of E_{adh} (Fig. 7). There is no overlap between the bonding charge densities of neighboring cells.

The calculated Bader charges on the Au_n clusters are shown in Figs. 8 and 9. All clusters considered gain electron charge; i.e., they are negatively charged. For a gold monomer the amount of accumulated electron charge is approximately the same as that typical for the Au_n rows (Fig. 3). For larger clusters the charging of Au atoms is twice as large as that of the Au_n rows. For $n=2-12$ clusters it varies between 1.04 and $1.18e$, with the exception of Au_5 and Au_7 where it amounts to 1.57 and $0.83e$, respectively. In the former, flat structure, the important electron donors are two Ti($5c$) atoms of the basal substrate layer, which add extra $\sim 0.4e$ to that characteristic of the Au_3 structure. The reason for a much smaller charge gain on the Au_7 cluster configuration (Fig. 9) is not clear. The major part of the electron-charge gain is localized on the three Au atoms sitting above the row of O^{br} vacancy sites (83% for Au_4, 75% for Au_5, 88% for Au_7, and 91%–95% for the Au_6 and Au_8-Au_{12} clusters) and is respon-

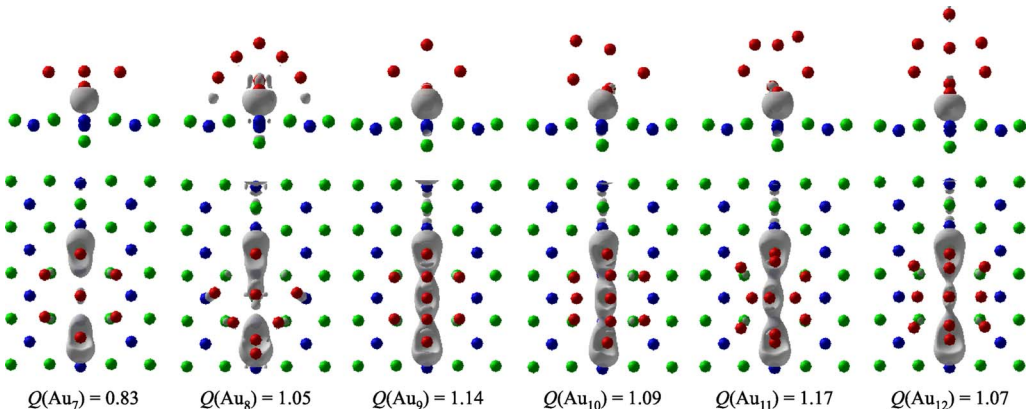

FIG. 9. (Color online) Same as in Fig. 8 but for $n=7-12$ gold clusters.

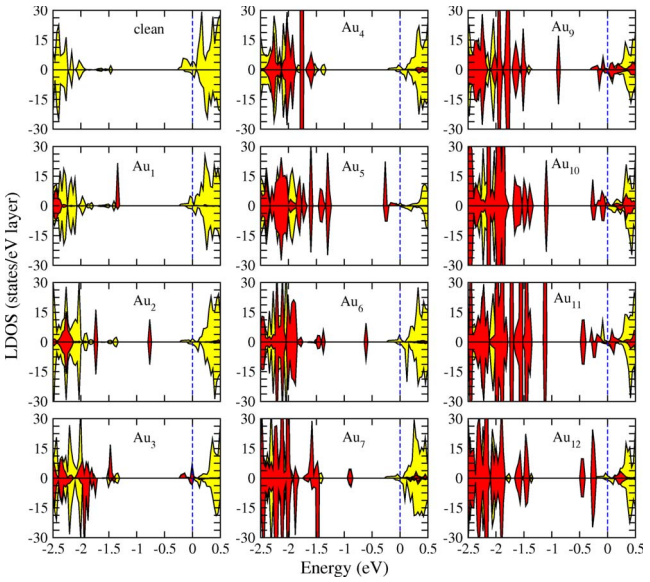

FIG. 10. (Color online) The local density of states for Au_n clusters on the defected $TiO_2(110)$ surface. Only the energy range close to the Fermi level (set as zero) is shown. The density of states of the top $TiO_2(110)$ 4×2 layer is plotted in yellow (gray), while red (dark gray) color marks the LDOS of Au clusters.

sible for the much stronger adhesive bonding of Au clusters than rows (cf. Figs. 2 and 7). Depending on the structure, the electron-charge gain of the central atom of the three Au atoms adsorbed in the O^{br} vacancy sites is two to five times smaller than on the outer atoms of this basal structure. In all cases the main part of the electron charge is donated by the Ti($6c$) atoms below the O^{br} vacancies. Another important but distinctly smaller ($\sim$3 times) part of the electron charge is donated to gold by the O($3c$) atoms lying in the basal TiO_2 plane on the two sides of the vacancy-line defect. The charging depends only little on odd or even number of Au atoms forming a cluster, in general, being $\sim$5–10% smaller for the even atom structures. The amount of charge transferred to a cluster correlates with the work function (see Fig. 7).

Figure 10 displays the local density of states on Au_n clusters ($n=1-7,9-12$) and on the Ti and O atoms of the top TiO_2 trilayer of the 4×2 surface cell. In order to facilitate their comparison with the results for Au_n rows (Fig. 4), they are plotted for the same energy window around the Fermi level. The presence of O^{br} vacancies on the clean $TiO_2(110)$ surface makes the states at the bottom of the conduction band to become occupied. However, the LDOS plots for the adsorbed gold clusters differ completely from those for the Au rows. In contrast to adsorption of the Au rows, which leads to the disappearance of the energy gap (cf. Fig. 4), Au clusters of $n=1-7$ atoms adsorbed on the defected $TiO_2(110)$ induce only very localized states in the energy gap. This changes only little for the higher gold isomers ($n=8-12$), and the energy gap does not disappear even for the largest cluster. Furthermore, in contrast to the findings of Ref. 22, for the $n\leq4$ clusters adsorbed on the single-vacancy defected surface, we see that the spins of the odd-numbered clusters remain unpaired, like in gas phase clusters. This should be connected with the higher reduction in our surface resulting in a single O^{br} atom that separates the adsorbed clusters from the neighboring cells. The unpaired spins of the odd-numbered clusters make that the cohesive energy and the work function of Au_n clusters oscillate with n (Fig. 7), in analogy to the electron affinity and the ionization potential of free Au clusters.

For even-numbered clusters ($n\geq4$) the Au bands are shifted more to lower energies than for the odd-numbered clusters (cf. Fig. 10). The analysis of the l-decomposed states (not shown) indicates that the single peak that appears for $n\leq3$ in the energy range between -1.5 eV and the Fermi level is predominantly of s character with a substantial contribution of d electrons. This $6s$ state moves far below the Fermi level (1.3–1.5 eV) compared to its position in the gas phase.[22] The stronger interaction and bonding between Au and the substrate Ti atoms at the trivacancy defected surface make the band shift for the Au monomer larger by about 1 eV than in the case of Au_1 adsorption at a single O^{br} vacancy.[22] In the Au_2 cluster the $6s$ state moves back toward the Fermi level by about 0.6 eV; for Au_3 it is shifted again toward lower energies (-1.5 eV). The latter and the two smaller peaks of $6s$ and $5d$ character which appear at the Fermi level overlap with the eigenstates of $TiO_2(110)$. For $n=4$ all these peaks disappear, to reappear in $n\geq5$ clusters, in the energy range between -1 and 0.5 eV, showing equal contribution from gold $6s$ and $5d$ states. In the largest clusters, $n\geq9$, there is an increasing density of states in the vicinity of the Fermi level, which manifests the increasing metallic character of the clusters.

IV. SUMMARY

The density-functional theory and PAW method were applied to study the optimum structure and energetics of Au rows and clusters on the defected $TiO_2(110)$ surfaces. We calculated structure and energetics of Au_n nanorows consisting of up to seven atoms and clusters formed of 1 to 12 atoms, adsorbed on the defected (110) rutile surface. The results show that both Au_n rows and clusters bind strongly to a defected TiO_2 surface. The adhesive binding energy of rows to the missing-row defected support is about 1.5 eV. The cohesive binding energy of Au atoms in the rows is about 2.5 eV/atom and does not show any specific trend with respect to the number of atoms that constitute the row. The analysis of the electron-charge-density distribution and the LDOS on gold rows points to their metallic nature. The calculated Bader charges show that all Au_n rows are negatively charged compared to the free standing structures.

The bonding of gold clusters to the defected $TiO_2(110)$ surface is of covalent nature and for the calculational setup considered in this work is stronger than that of Au rows. The cohesive energy per atom in the Au_n clusters is about the same as that in the Au rows. The analysis of calculated Bader charges shows that Au clusters on the defected $TiO_2(110)$ surface are negatively charged with the electron charge transferred mainly from the Ti($6c$) atoms, which is left behind by the removed bridging oxygen atoms. The amount of charge transferred to the clusters is approximately twice as large as

to the rows. The electron charge on the cluster, its cohesive energy, and the work function exhibit weak dependence on the odd-even number of gold atoms forming the cluster.

ACKNOWLEDGMENTS

We would like to thank Ernst Bauer for his interest in this research and useful comments on this work. Part of the calculations were performed at the Interdisciplinary Centre for Mathematical and Computational Modeling (ICM) of the Warsaw University under the Research Project No. G28-25. A.K. acknowledges the access to high performance computers of the EPCC Edinburgh within the HPC-EUROPA project (RII3-CT-2003-506079), with the support of the European Community – Research Infrastructure Action under the FP6 Programme.

*Corresponding author; kiejna@ifd.uni.wroc.pl

[1] M. Haruta, N. Yamada, T. Kobayashi, and S. Iijima, J. Catal. **115**, 301 (1989).
[2] M. Valden, X. Lai, and D. W. Goodman, Science **281**, 1647 (1998).
[3] M. S. Chen and D. W. Goodman, Science **306**, 252 (2004).
[4] M. Haruta, Chem. Rec. **3**, 75 (2003).
[5] N. Lopez and J. K. Nørskov, J. Am. Chem. Soc. **124**, 11262 (2002).
[6] N. Lopez, T. V. W. Janssens, B. S. Clausen, Y. Xu, M. Mavrikakis, T. Bligaard, and J. K. Nørskov, J. Catal. **223**, 232 (2004).
[7] Z. P. Liu, X. Q. Gong, J. Kohanoff, C. Sanchez, and P. Hu, Phys. Rev. Lett. **91**, 266102 (2003).
[8] L. M. Molina, M. D. Rasmussen, and B. Hammer, J. Chem. Phys. **120**, 7673 (2004).
[9] L. Thiên-Nga and A. T. Paxton, Phys. Rev. B **58**, 13233 (1998).
[10] Z. Yang, R. Wu, and D. W. Goodman, Phys. Rev. B **61**, 14066 (2000).
[11] L. Giordano, G. Pacchioni, T. Bredow, and J. F. Sanz, Surf. Sci. **471**, 21 (2001).
[12] N. Lopez and J. K. Nørskov, Surf. Sci. **515**, 175 (2002).
[13] M. V. Ganduglia-Pirovano, A. Hofmann, and J. Sauer, Surf. Sci. Rep. **62**, 219 (2007).
[14] Y. Wang and G. S. Hwang, Surf. Sci. **542**, 72 (2003).
[15] A. Vijay, G. Mills, and H. Metiu, J. Chem. Phys. **118**, 6536 (2003).
[16] E. Wahlström, N. Lopez, R. Schaub, P. Thostrup, A. Rønnau, C. Africh, E. Lægsgaard, J. K. Nørskov, and F. Besenbacher, Phys. Rev. Lett. **90**, 026101 (2003).
[17] N. Lopez, J. K. Nørskov, T. V. W. Janssens, A. Carlsson, A. Puig-Molina, B. S. Clausen, and J.-D. Grunwaldt, J. Catal. **225**, 86 (2004).
[18] K. Okazaki, Y. Morikawa, S. Tanaka, K. Tanaka, and M. Kohyama, Phys. Rev. B **69**, 235404 (2004).
[19] H. Iddir, S. Öğüt, N. D. Browning, and M. M. Disko, Phys. Rev. B **72**, 081407(R) (2005).
[20] I. N. Remediakis, N. Lopez, and J. K. Nørskov, Angew. Chem., Int. Ed. **44**, 1824 (2005).
[21] S. N. Rashkeev, A. R. Lupini, S. H. Overbury, S. J. Pennycook, and S. T. Pantelides, Phys. Rev. B **76**, 035438 (2007).
[22] D. Pillay and G. S. Hwang, Phys. Rev. B **72**, 205422 (2005).
[23] A. Locatelli, T. Pabisiak, A. Pavlovska, T. O. Mentes, L. Aballe, A. Kiejna, and E. Bauer, J. Phys.: Condens. Matter **19**, 082202 (2007).
[24] T. O. Menteş, A. Locatelli, L. Aballe, A. Pavlovska, E. Bauer, T. Pabisiak, and A. Kiejna, Phys. Rev. B **76**, 155413 (2007).
[25] S. J. Thompson and S. P. Lewis, Bull. Am. Phys. Soc. **52** (2007), http://meetings.aps.org/link/BAPS.2007.MAR.V42.10
[26] S. Chrétien and H. Metiu, J. Chem. Phys. **126**, 104701 (2007).
[27] S. Chrétien and H. Metiu, J. Chem. Phys. **127**, 244708 (2007).
[28] S. Chrétien and H. Metiu, J. Chem. Phys. **127**, 084704 (2007).
[29] J. G. Wang and B. Hammer, Phys. Rev. Lett. **97**, 136107 (2006).
[30] D. Matthey, J. G. Wang, S. Wendt, J. Matthiesen, R. Schaub, E. Lægsgaard, B. Hammer, and F. Besenbacher, Science **315**, 1692 (2007).
[31] G. Kresse and J. Hafner, Phys. Rev. B **47**, 558 (1993).
[32] G. Kresse and J. Furthmüller, Phys. Rev. B **54**, 11169 (1996); Comput. Mater. Sci. **6**, 15 (1996).
[33] J. P. Perdew, K. Burke, and M. Ernzerhof, Phys. Rev. Lett. **77**, 3865 (1996).
[34] G. Kresse and D. Joubert, Phys. Rev. B **59**, 1758 (1999).
[35] P. E. Blöchl, Phys. Rev. B **50**, 17953 (1994).
[36] A. Kiejna, T. Pabisiak, and S. Gao, J. Phys.: Condens. Matter **18**, 4207 (2006).
[37] H. J. Monkhorst and J. D. Pack, Phys. Rev. B **13**, 5188 (1976).
[38] R. F. W. Bader, *Atoms in Molecules: A Quantum Theory* (Oxford University Press, Oxford, 1990).
[39] G. Henkelman, A. Arnaldsson, and H. Jónsson, Comput. Mater. Sci. **36**, 354 (2006).
[40] A. Kiejna, Phys. Rev. B **74**, 235429 (2006).
[41] T. Okazawa, M. Kohyama, and Y. Kido, Surf. Sci. **600**, 4430 (2006).
[42] T. Pabisiak and A. Kiejna, Solid State Commun. **144**, 324 (2007).
[43] V. E. Henrich and P. A. Cox, *The Surface Science of Metal Oxides* (Cambridge University Press, Cambridge, 1994).
[44] L. Xiao, B. Tollberg, X. Hu, and L. Wang, J. Chem. Phys. **124**, 114309 (2006).
[45] L. M. Molina and J. A. Alonso, J. Phys. Chem. C **111**, 6668 (2007).
[46] P. Frondelius, H. Häkkinen, and K. Honkala, New J. Phys. **9**, 339 (2007).
[47] J. P. Perdew, J. A. Chevary, S. H. Vosko, K. A. Jackson, M. R. Pederson, D. J. Singh, and C. Fiolhais, Phys. Rev. B **46**, 6671 (1992).
[48] D. Pillay and G. S. Hwang, J. Mol. Struct.: THEOCHEM **771**, 129 (2006).
[49] W. A. de Heer, Rev. Mod. Phys. **65**, 611 (1993).